Supporting Information

On Synapse Intelligence Emulated in A Self-formed Artificial Synaptic Network

*B. Bharath and Giridhar U. Kulkarni**

Chemistry & Physics of Materials Unit and Thematic Unit of Excellence in Nanochemistry, Jawaharlal Nehru Centre for Advanced Scientific Research, Jakkur P.O., Bangalore 560064, India.

Experimental Section:

Ag-ASN preparation: Glass or SiO_2/Si substrate was sonicated in acetone and IPA for 5 min and dried under nitrogen. The substrate was then loaded to e-beam evaporator for Ag deposition. ~30 nm Ag was deposited at chamber vacuum of ~10^{-6} torr. Later the substrate was placed on a hot plate kept at 300 °C for 30 s and then immediately placed on a cold surface to obtain dewetted film.

Device fabrication: Au gap electrodes were fabricated by shadow masking technique.

Characterization: I-V characterization of the device was done using Keithley 2450, FESEM images were captured using Inspect F50 FESEM, atomic force microscope was performed under contact and conducting mode using Bruker Innova AFM, HRTEM study was done using FEI TALOS F200S G2, X-ray diffraction (XRD) study was carried out using Rigaku diffractometer, temperature dependent resistance measurement was done using Linkam temperature stage, X-ray photoelectron (XP) spectra were recorded using an Omicron nanotechnology spectrometer with Mg Kα X-ray source (E = 1253.6 eV).

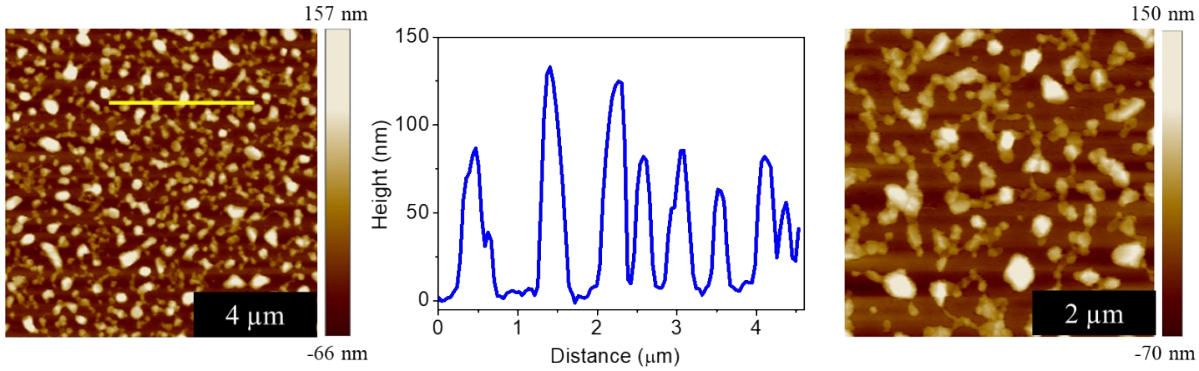

Fig. S1: Low and high magnification contact mode AFM imaging of the annealed film. The average surface roughness was found to be ~35 nm. Height profile along the yellow line is shown.

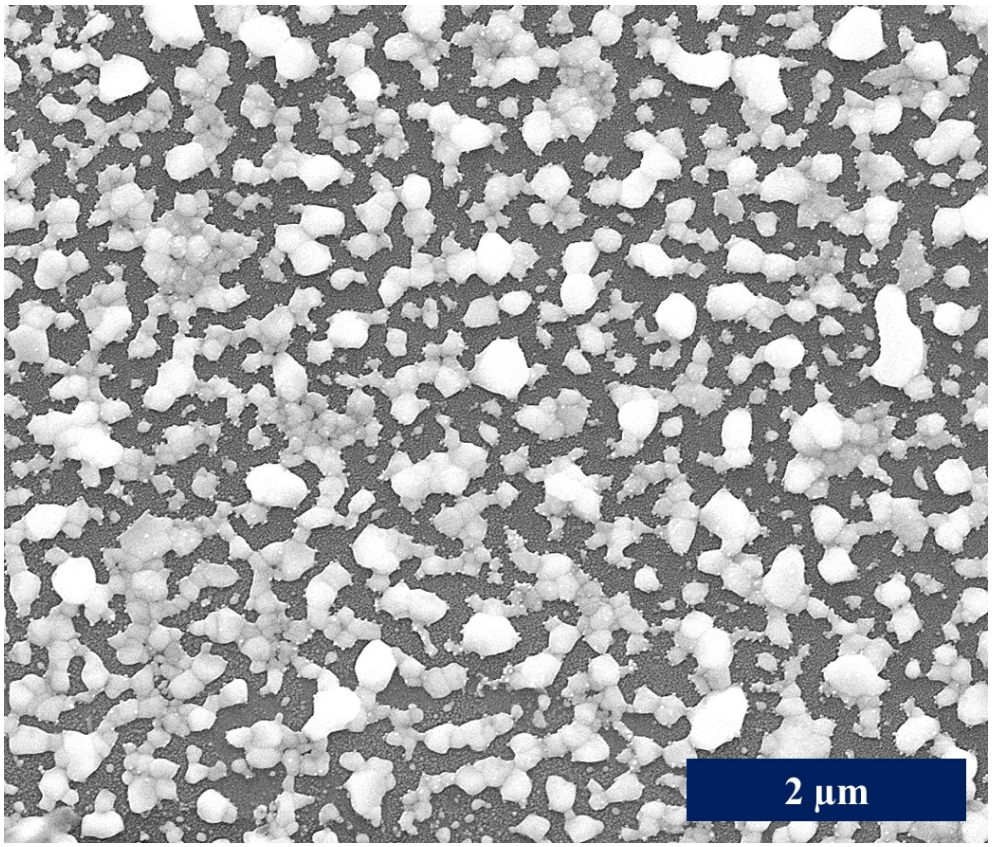

Fig. S2: SEM image of the annealed film showing the presence of colossal nanogaps between the agglomerates.

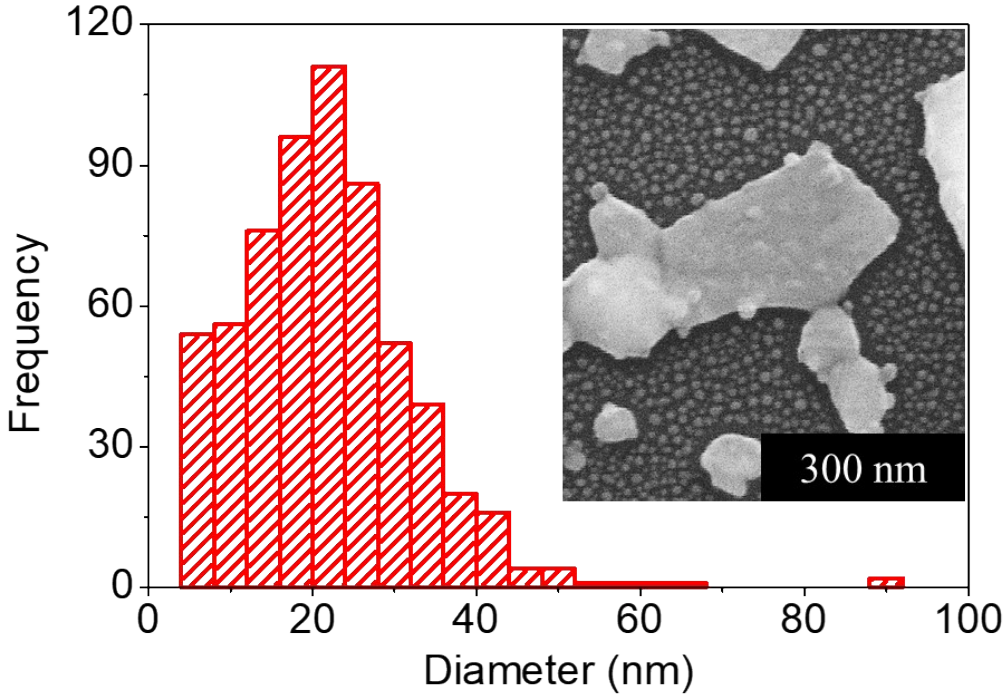

Fig. S3: Size distribution of the small Ag particles (inset) present in between the agglomerates.

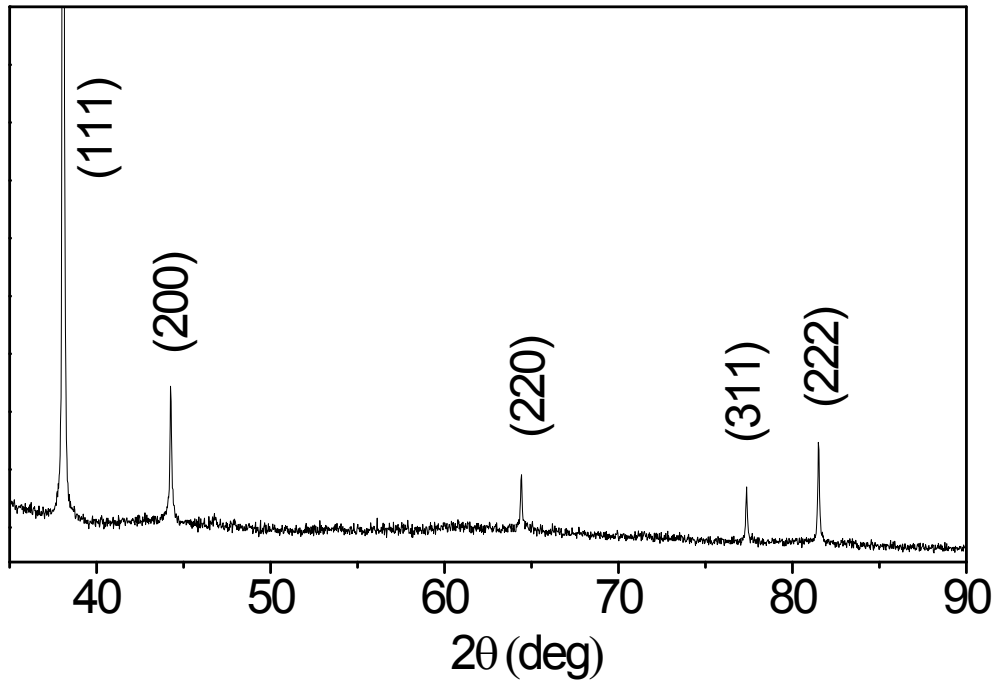

Fig. S4: XRD pattern of the annealed film on glass showing the dominant (111) peak with no detectable oxidation.

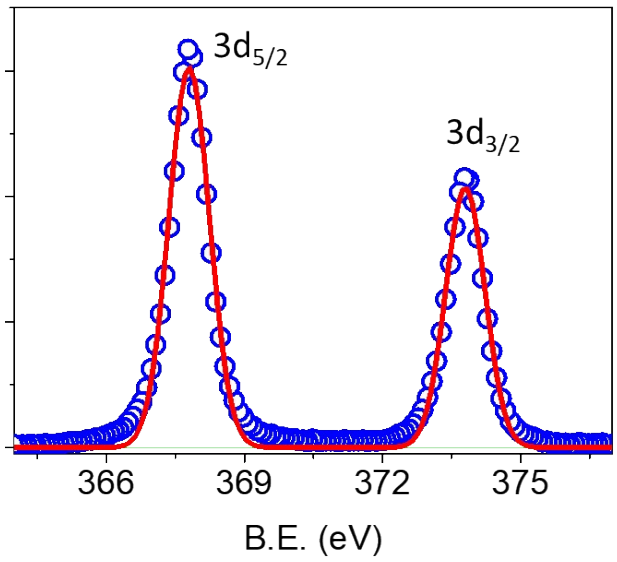

Fig. S5: Core level XP spectra in Ag 3d region. The shift (-0.4 eV) in the peak position is due to the mild surface oxidation.

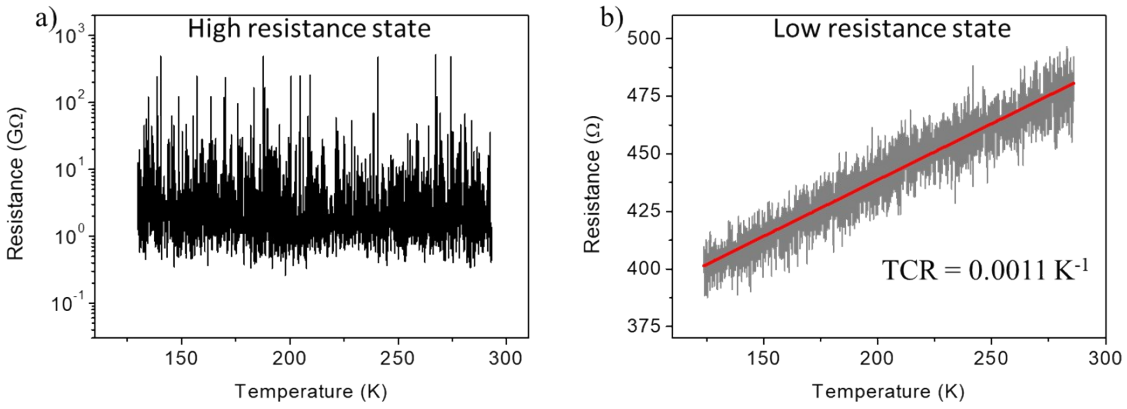

Fig. S6: Temperature dependent electrical resistance of the device. a) Temperature independent resistance reflects the tunnelling type conduction in high resistance state. b) Linear increase in low resistance state with temperature indicates the metallic nature of the conduction filaments. Bias voltage was 100 mV.

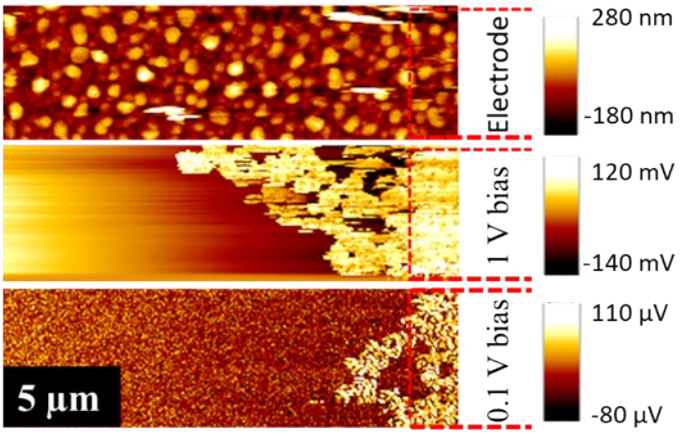

Fig. S7: Conducting AFM measurement was performed to realize the conduction path created in the device during electrical bias. Top figure shows the contact mode topography image of the device. For CAFM bias, the electrode was connected to ground and the tip was biased. When the tip was biased at 1 V, conduction path appeared due to the electromigration of Ag to bridge the nanogap. Due to the short-term stability these filaments relax back and when scanned with 0.1 V tip bias, majority of the conduction paths were vanished except for those near the electrode.

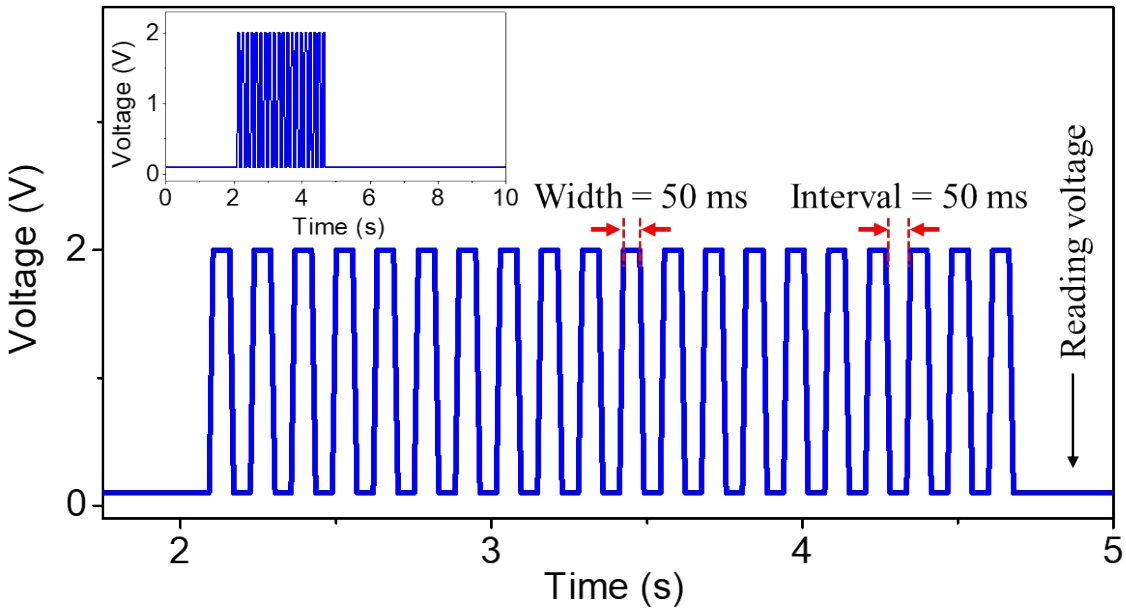

Fig. S8: Pulse configuration. 20 pulses of 2 V amplitude and 50 ms width as well as interval with 0.1 V reading voltage.

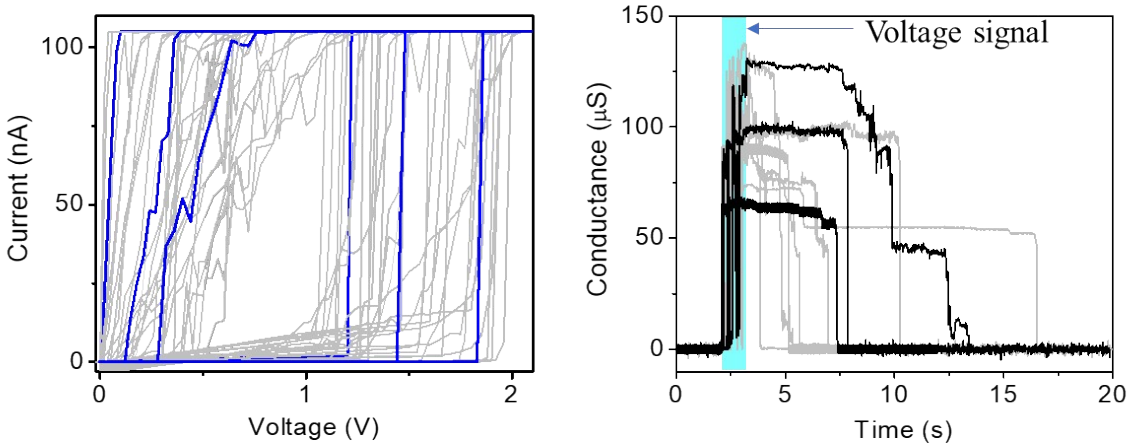

Fig. S9: Over 30 batches of samples were prepared for the fabrication of synaptic devices to validate the reproducibility. All showed highly reproducible synaptic behavior. I-V switching and STP characteristics of some devices are shown here.

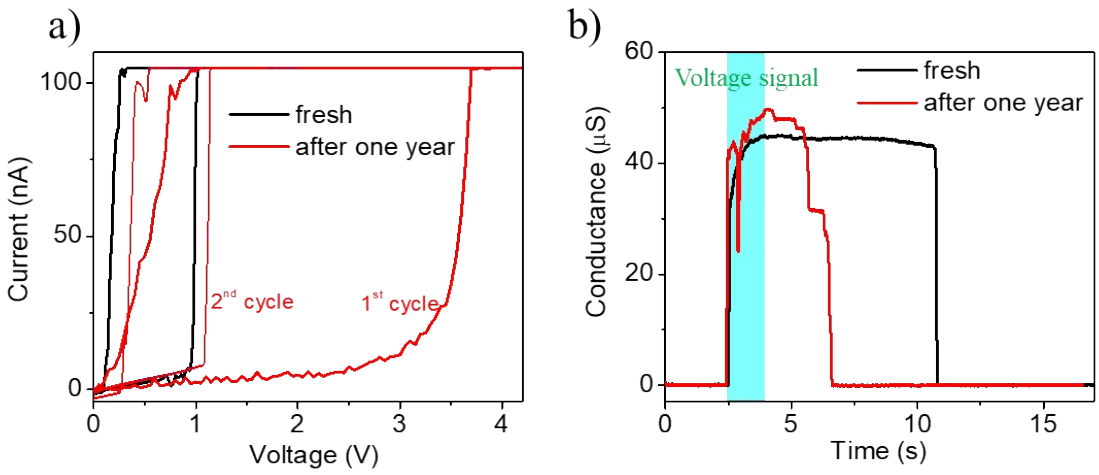

Fig. S10: Device stability, a) After a year of fabrication, the device switching voltage was seen shifted to a higher value (1st cycle) possibly due to the mild surface oxidation. However, the device recovered to its pristine state during the subsequent I-V cycle (2nd cycle) which may be attributed to joule heating leading to decomposition of oxide formation.[41] b) STP behavior was reproducible even in the aged device.

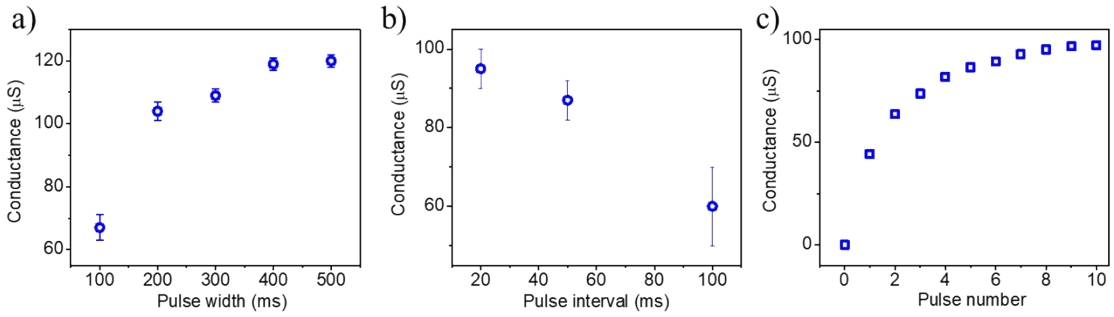

Fig. S11: Conductance modulation with a) pulse width (single pulse with 2 V amplitude), b) pulse interval (20 x 2 V pulses with 50 ms width) and c) pulse number (2 V pulse with 50 ms width).

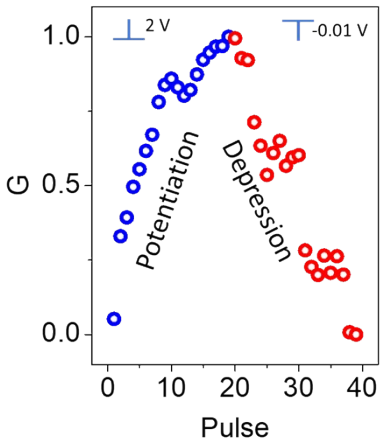

Fig. S12: Potentiation and depression. 20 potentiation pulse and 20 depression pulse were applied to show the tunability of conductance. Pulse width was 50 ms.

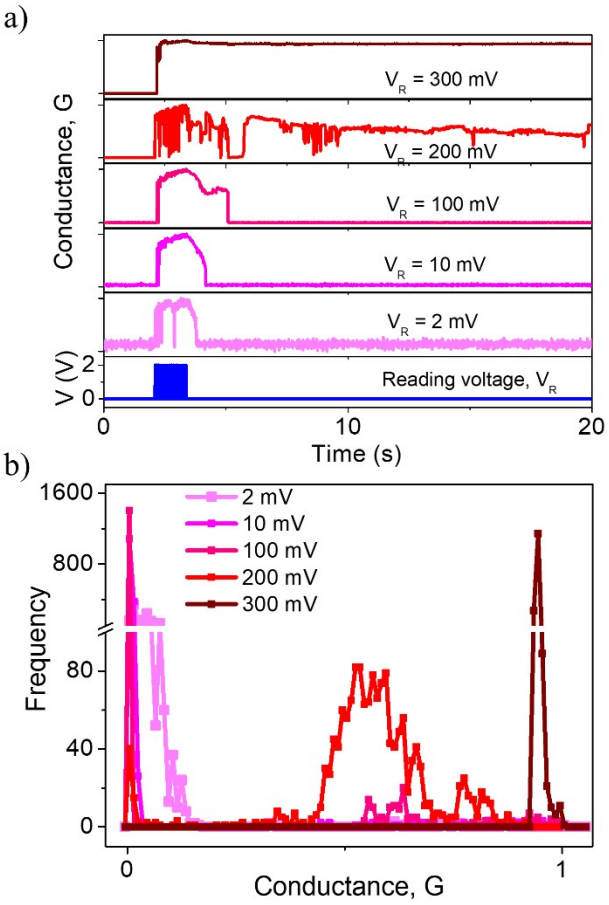

Fig. S13: a) Memristor behavior under different supervising voltages. b) Distribution of conductance for different supervising voltages. Frequency here represents the instances (counts) of achieved conductance value (junior's behavior) attained by the device after pulse signal or during the supervision voltage. During low supervision voltages (2-100 mV), maximum (peak) count is appearing at low conductance value suggesting that the junior tends to be lazy while under strict supervision (300 mV), the count is maximum for high conductance value representing full attentiveness. However,

during moderate supervision (200 mV), there are two peaks at both high and low conductance values suggesting intermittent attentiveness.

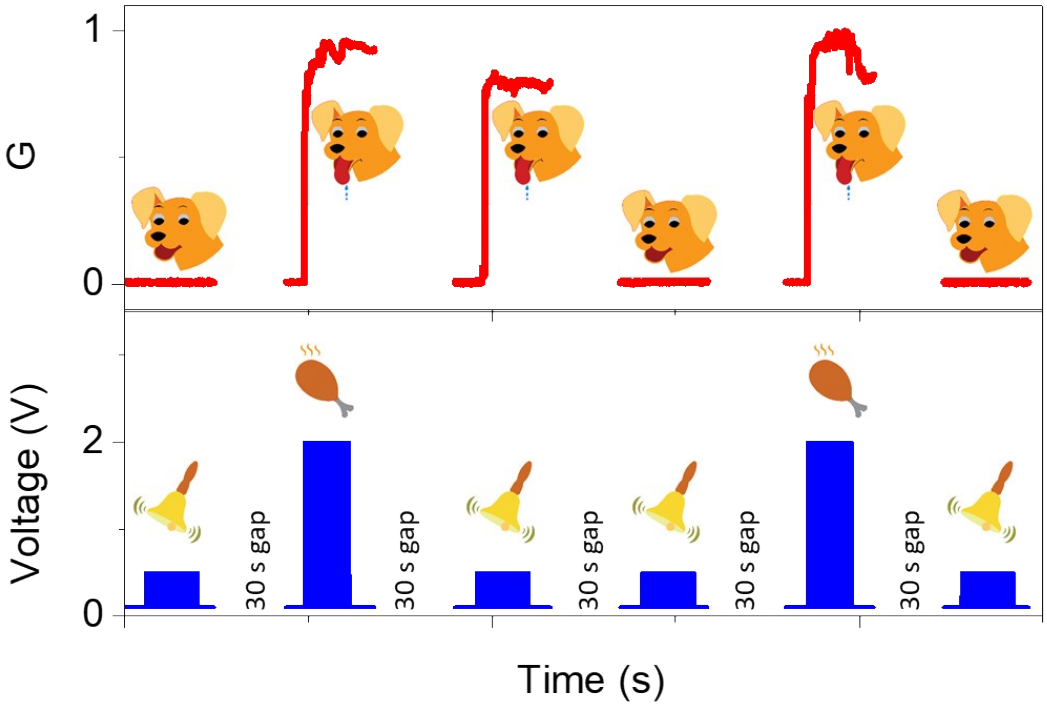

Fig. S14: Dissociation of the classical conditioning. Here, after the extinction, the device did not respond to the bell signal. The food signal was then applied without the bell signal and the device responded. Because of the previous association, the device could respond to the immediate bell signal but not to the latter signals as this behavior decayed. However, the device continued to respond to the food signal without the bell signal. As there was no association between the food and bell signals, interestingly, the device did not respond to the following bell signal (illustrating complete dissociation). A 30 s gap was observed after each stage.

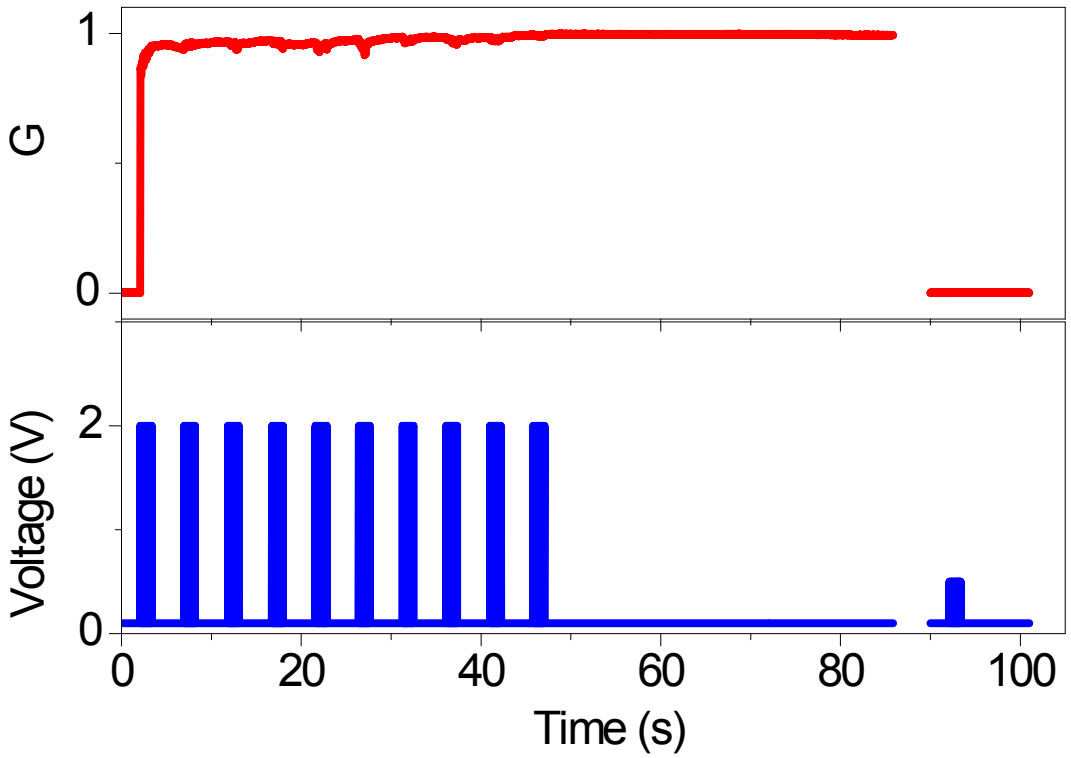

Fig. S15: Only food pulse is applied for 10 cycles without bell pulse. The device showed response for the food. Now a bell pulse is applied to check whether the device will respond due to previous large number of food cycle. But it can be seen that the device did not respond to the bell pulse. This clearly shows that food must be accompanied with bell pulse to create association.

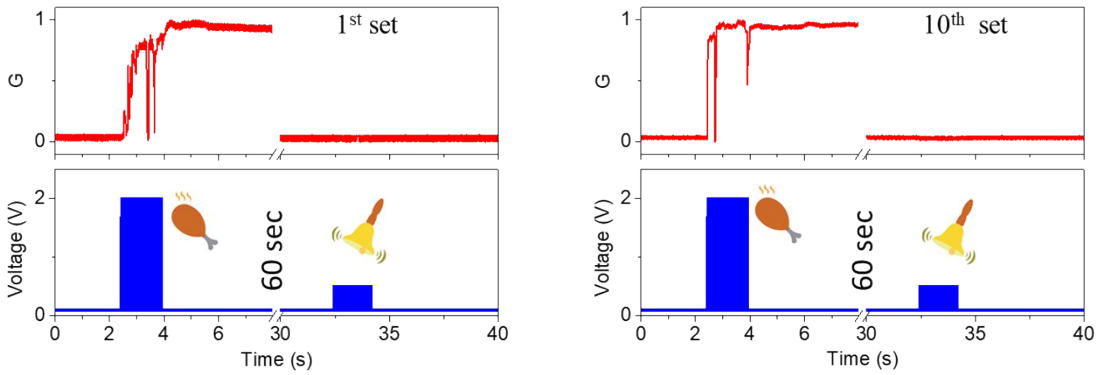

Fig. S16: Large gap between food and bell signals will not be able to create the association. Here the food and bell signals were applied with a large gap of 60 sec. Even after 10 sets of such pulse sequence, the device shows no response to the bell signal displaying no association.

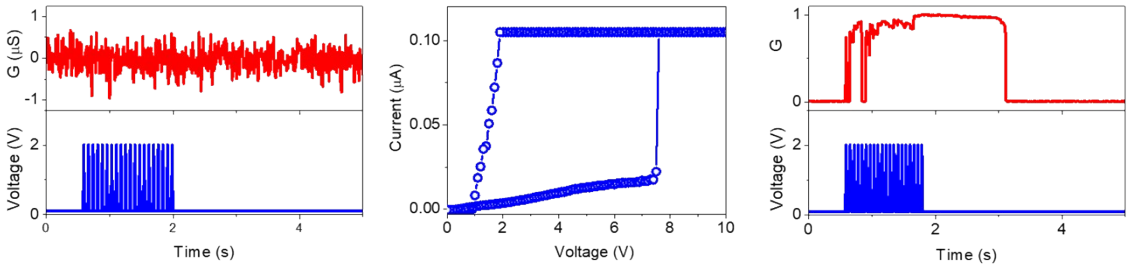

Fig. S17: Observation of synaptic fatigue and recovery. Due to colossal learning cycle (> 10^4), the device did not respond undergoing fatigue which is similar to the biological synapse. To reactivate, the device was treated with voltage sweep at higher voltage range where it recovers the switching behavior. Further, under the application of voltage pulses, the device starts responding displaying the synaptic recovery. (20 pulses of 2 V, 50 ms width as well as interval, 100 mV reading voltage).

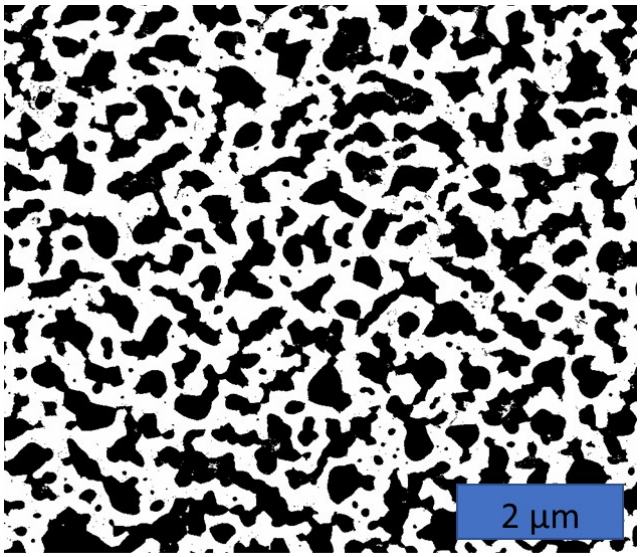

Fig. S18: SEM image was analysed using ImageJ and average agglomerate density was found to be around 1.1 × 10^9 per square inch. Considering average 5 nanogap-like synapse per agglomerate, average synapse density will be 5.5 × 10^9 per square inch. Bio neural network has approximately 1.28 × 10^{13} synapses per cubic inch. Considering average size of a neuron, in-plane synapse density will be around ~10^9 per square inch.

Table S1: Synaptic performance comparison of multi-terminal devices from the literature. Advanced behavioral patterns can be emulated either using hardware-based configuration or using software based neural networks. Here, only hardware based behavioral studies are considered for comparison.

Material	Supporting circuit	Signal	STP	LTP	P / D	Supervision / impression of supervision	Interest/ mood based learning	Associative learning	Synaptic fatigue and recovery	Ref
ITO/Nb:$SrTiO_3$/ITO	-	O	✓	✓	-	-	✓	-	-	1
ITO/Al_2O_3/PI/Ag	-	E	-	-	-	-	-	✓	-	2
Pt/FeO_x/SiO_2/Pt	✓	E	-	-	-	-	-	✓	-	3
Ni/NiOx/Ni/Au	✓	E	-	✓	-	-	-	✓	-	4
Pt/$Ge_{0.3}Se_{0.7}$/SiO_2/ Cu	✓	E	-	-	-	-	-	✓	-	5
Au NPs/ pentacene	✓	E	-	-	-	-	-	✓	-	6
Pt/Ag/SiO_x:Ag/Ag/ Pt + Pt/Ta_2O_5/TaO_x/ Pt	✓	E	-	-	-	-		✓	-	7
ITO/ Chitosan /ITO	-	E	-	-	✓	-	-	✓	-	8
ITO/ PEDOT:PSS/ CuSCN/ $CsPbBr_3$PNs/Au	-	O + E	✓	✓	✓	-	-	-	-	9
Mo/CdS/ ZTO/Mo	-	O	✓	✓	-	-	-	✓	-	10
Au/PMMA/$MAPbI_3$/ Si NM/SiO_2/ Si	-	O	✓	✓	-	-	✓	-	-	11
ITO/PCBM/ $MAPbI_3$:SiNCs/ Spiro-OMeTAD/Au	-	O	✓	-	-	-	-	-	-	12
poly-Si/SiO_2/Si_3N_4/ SiO_2/Si	-	E	✓	✓	✓	-	-	-	✓	13
Au/$La_{1.875}Sr_{0.125}NiO_4$/ Au	-	O	✓	✓	-	-	-	-	-	14
Au/IGZO/alkylated GO/ion gel/ Au	-	O + E	✓	✓	✓	-	-	-	-	15
Au/WS_2/ PZT/Au	-	O + E	✓	✓	✓	-	-	-	-	16
Pt/TiN/ $Pr_{0.7}Ca_{0.3}MnO_3$/Pt	✓	E	-	-	✓	-	-	✓	-	17
Au/Ag-ASN/Au	**-**	**E**	✓	✓	✓	✓	✓	✓	✓	**This work**

O = Optical, E = Electrical, P = Potentiation, D = Depression

References:

1 S. Gao, G. Liu, H. Yang, C. Hu, Q. Chen, G. Gong, W. Xue, X. Yi, J. Shang and R. W. Li, *ACS Nano*, 2019, **13**, 2634–2642.

2 C. Wu, T. W. Kim, T. Guo, F. Li, D. U. Lee and J. J. Yang, *Adv. Mater.*, 2017, **29**, 1602890.

3 X. Wan, D. Liang, F. Gao, X. Lian and Y. Tong, *Appl. Phys. Express*, 2018, **11**, 114601.

4 S. G. Hu, Y. Liu, Z. Liu, T. P. Chen, Q. Yu, L. J. Deng, Y. Yin and S. Hosaka, *J. Appl. Phys.*, 2014, **116**, 214502.

5 M. Ziegler, R. Soni, T. Patelczyk, M. Ignatov, T. Bartsch, P. Meuffels and H. Kohlstedt, *Adv. Funct. Mater.*, 2012, **22**, 2744–2749.

6 O. Bichler, W. Zhao, F. Alibart, S. Pleutin, S. Lenfant, D. Vuillaume and C. Gamrat, *Neural Comput.*, 2013, **25**, 549–566.

7 Z. Wang, M. Rao, J. W. Han, J. Zhang, P. Lin, Y. Li, C. Li, W. Song, S. Asapu, R. Midya, Y. Zhuo, H. Jiang, J. H. Yoon, N. K. Upadhyay, S. Joshi, M. Hu, J. P. Strachan, M. Barnell, Q. Wu, H. Wu, Q. Qiu, R. S. Williams, Q. Xia and J. J. Yang, *Nat. Commun.*, 2018, **9**, 8409.

8 F. Yu, L. Q. Zhu, H. Xiao, W. T. Gao and Y. B. Guo, *Adv. Funct. Mater.*, 2018, **28**, 1804025.

9 F. Ma, Y. Zhu, Z. Xu, Y. Liu, X. Zheng, S. Ju, Q. Li, Z. Ni, H. Hu, Y. Chai, C. Wu, T. W. Kim and F. Li, *Adv. Funct. Mater.*, 2020, **30**, 1908901.

10 S. W. Cho, S. M. Kwon, M. Lee, J. W. Jo, J. S. Heo, Y. H. Kim, H. K. Cho and S. K. Park, *Nano Energy*, 2019, **66**, 104097.

11 L. Yin, W. Huang, R. Xiao, W. Peng, Y. Zhu, Y. Zhang, X. Pi and D. Yang, *Nano Lett.*, 2020, **20**, 3378−3387.

12 W. Huang, P. Hang, Y. Wang, K. Wang, S. Han, Z. Chen, W. Peng, Y. Zhu, M. Xu, Y. Zhang, Y. Fang, X. Yu, D. Yang and X. Pi, *Nano Energy*, 2020, **73**, 104790.

13 J. Hur, B. C. Jang, J. Park, D. Il Moon, H. Bae, J. Y. Park, G. H. Kim, S. B. Jeon, M. Seo, S. Kim, S. Y.

Choi and Y. K. Choi, *Adv. Funct. Mater.*, 2018, **28**, 1804844.

14 L. Zhao, Z. Fan, S. Cheng, L. Hong, Y. Li, G. Tian, D. Chen, Z. Hou, M. Qin, M. Zeng, X. Lu, G. Zhou, X. Gao and J. M. Liu, *Adv. Electron. Mater.*, 2020, **6**, 1900858.

15 J. Sun, S. Oh, Y. Choi, S. Seo, M. J. Oh, M. Lee, W. B. Lee, P. J. Yoo, J. H. Cho and J. H. Park, *Adv. Funct. Mater.*, 2018, **28**, 1804397.

16 Z. D. Luo, X. Xia, M. M. Yang, N. R. Wilson, A. Gruverman and M. Alexe, *ACS Nano*, 2020, **14**, 746–754.

17 K. Moon, S. Park, J. Jang, D. Lee, J. Woo, E. Cha, S. Lee, J. Park, J. Song, Y. Koo and H. Hwang, *Nanotechnology*, 2014, **25**, 495204.